



HAL
open science

A strong seismic velocity contrast in the shallow mantle across the Zagros collision zone (Iran)

A. Kaviani, Anne Paul, E. Bourova, Denis Hatzfeld, Helle Pedersen, M.
Mokhtari

► **To cite this version:**

A. Kaviani, Anne Paul, E. Bourova, Denis Hatzfeld, Helle Pedersen, et al.. A strong seismic velocity contrast in the shallow mantle across the Zagros collision zone (Iran). *Geophysical Journal International*, 2007, 171, pp.399-410. 10.1111/j.1365-246X.2007.03535.x . hal-00195522v1

HAL Id: hal-00195522

<https://hal.science/hal-00195522v1>

Submitted on 11 Dec 2007 (v1), last revised 23 Nov 2020 (v2)

HAL is a multi-disciplinary open access archive for the deposit and dissemination of scientific research documents, whether they are published or not. The documents may come from teaching and research institutions in France or abroad, or from public or private research centers.

L'archive ouverte pluridisciplinaire **HAL**, est destinée au dépôt et à la diffusion de documents scientifiques de niveau recherche, publiés ou non, émanant des établissements d'enseignement et de recherche français ou étrangers, des laboratoires publics ou privés.

A strong seismic velocity contrast in the shallow mantle across the Zagros collision zone (Iran)

A. Kaviani ^{1,2}, A. Paul ¹, E. Bourova ¹, D. Hatzfeld ¹, H. Pedersen ¹, M. Mokhtari ²

¹ *Laboratoire de Géophysique Interne et Tectonophysique, CNRS & Université Joseph Fourier, P. O. Box 53, 38041 Grenoble, France*

² *International Institute of Earthquake Engineering and Seismology (IIEES), P. O. Box 19395/3913, Tehran, Iran*

Revised version, 8 June 2007

Keywords: Zagros collision belt, lithospheric structure, teleseismic tomography, surface wave dispersion

Abstract

Surface-wave dispersion measurements are interpreted jointly with the inversion of teleseismic P wave traveltimes along a dense 620-km long temporary seismic profile across the Zagros to investigate its upper mantle structure. The S-wave model determined from Rayleigh wave dispersion in the Zagros fold-and-thrust belt has high velocities from $4.5 \pm 0.2 \text{ km.s}^{-1}$ below the Moho to $4.9 \pm 0.25 \text{ km.s}^{-1}$ at 200 km depth, which are comparable to a shield-like structure. Beneath the suture region from the Main Zagros Thrust to the Urumieh-Dokhtar volcanic arc, S-wave velocities are lower than beneath the Zagros in the top 50 km of the upper mantle, with a minimum of $4.4 \pm 0.2 \text{ km.s}^{-1}$ at 80 km depth. From 150 km and deeper, S velocities are as high as beneath the Zagros. We suggest that part of the velocity difference at shallow depth is due to higher mantle temperatures and/or higher fluid content beneath the northern half of the profile, but that velocities are too high to support the hypothesis of mantle lid delamination under the suture zone. Teleseismic P traveltimes relative residuals display a long-wavelength variation along the transect, with a difference of 1.1s between negative residuals in the Zagros Simple Folded Belt and positive residuals in Central Iran. This difference backprojects into a 6 to 7% lateral variation of P-wave velocity in the shallow upper mantle, with higher V_P beneath Zagros and lower V_P beneath Central Iran. The main short wavelength variation of the residual is located in the suture region, with late P arrivals in the region of the Main Zagros Thrust and early arrivals in the Sanandaj-Sirjan zone. Using synthetic models of V_P perturbations, we show that the high velocities of the Arabian platform have to extend laterally at least to the Sanandaj-Sirjan zone to fit the observed P delays. This model also predicts Rayleigh wave phase velocities which are within the error bars of the

observed dispersion. It supports the model of crustal-scale overthrusting at the Main Zagros Thrust.

Introduction

The Zagros mountain belt in southwestern Iran results from the collision of Arabia and Eurasia after the closure of the Neotethys oceanic domain in the Oligo-Miocene (Fig. 1a). This continental collision, young and of limited geographical extension, is a natural laboratory for investigating processes related to the early phases of mountain building. The role of continental subduction in the transition from oceanic subduction to continental collision (see modeling by Regard et al., 2003), the response of the lithospheric mantle to shortening (see modeling by Bird, 1978), or the role of lithospheric delamination in the formation of the Turkish-Iranian plateau (Maggi & Priestley, 2005) are still open questions. Previous studies of the Zagros region from regional data document differences in the seismic properties of the upper mantle beneath the Arabian platform and Central Iran (e.g. Maggi & Priestley, 2005). However, their resolution is too low to easily connect the observations with surface geology.

We here present the first tomography results across the Zagros belt based on a dense temporary seismic array. The 620-km long array (Fig. 1a) was installed in the area for a duration of 4½ months. In spite of the short duration of the experiment, and therefore the limited amount of data, we are able to give some constraints on upper mantle structure through a joint interpretation of surface wave dispersion and teleseismic *P*-wave tomography.

Tectonic setting

The Central Iranian micro-continent is constituted of separate continental blocks that detached from Gondwana in the Permian to early-Triassic and subsequently accreted onto Eurasia along the Alborz and Kopet-Dag sutures during the late Triassic closure of the Paleo-Tethys (Stöcklin, 1968; Falcon, 1974; Stoneley, 1981). The subduction of the Neo-Tethys Ocean beneath the southern margin of the Central Iranian blocks started by the Late Jurassic (e.g. Berberian & King, 1981), and the onset of the closure of the oceanic domain was marked by the obduction of ophiolites along the Main Zagros Thrust (MZT) in the Late Cretaceous (Agard et al., 2005). Still, it is not certain whether the calc-alkaline volcanism of the Sanandaj-Sirjan metamorphic zone (SSZ) and of the Urumieh-Dokhtar magmatic arc (UDMA) was related to subduction (see Berberian & King, 1981 and references herein).

Even though evidence from different sources indicates different times of closure of the Neotethys (hereafter called Tethys), the collision has been purely continental for at least 5 Ma (Stoneley, 1981; McQuarrie et al., 2003; Agard et al., 2005). The present velocity of Arabia with respect to Eurasia is approximately $22 \pm 2 \text{ mm.y}^{-1}$ in the direction $N8 \pm 5^\circ E$ (Vernant et al., 2004). This convergence is accommodated by crustal shortening by fold-and-thrust deformation in the Zagros, Alborz and Kopet-Dag and by lateral displacements of the blocks of Central Iran along major strike-slip faults.

The Zagros collision zone comprises three major sub-parallel tectonic elements with a general NW-SE trend. They are, from SW to NE, the Zagros Fold and Thrust Belt (ZFTB), the Sanandaj-Sirjan metamorphic zone (SSZ), and the Urumieh-Dokhtar Magmatic Arc (UDMA) (Stöcklin, 1968; Ricou et al., 1977) (Fig. 1b). The ZFTB is characterized by a sequence of Paleozoic and Mesozoic shelf sediments deposited on the subsiding Arabian continental margin. This sequence forms a 200-300 km wide simply folded range extending about 1200 km from eastern Turkey to the Strait of Hormuz (Berberian & King, 1981; Stoneley, 1981). The Main Zagros Reverse Fault or Main Zagros Thrust (MZT) (Stöcklin, 1968, 1974) marks the boundary between the ZFTB and the SSZ (Stöcklin, 1968, 1974; Ricou et al., 1977; Berberian, 1995). Recent geological (Agard et al., 2005) and geophysical (Paul et al., 2006) data suggest that the MZT is deeply rooted, possibly to Moho depths, and that it coincides with the suture between Arabia and the plate fragments that make up Iran. The 150-200-km wide SSZ has undergone various metamorphic episodes during the subduction of the Tethyan Ocean under the Iranian block, the obduction of ophiolites along the MZT, and the final continental collision (Stöcklin, 1968; Davoudzadeh et al., 1997). During this latest episode, the SSZ overthrust the Zagros sedimentary sequence along the MZT (Stöcklin, 1968; Agard et al., 2005). To the northeast, the UDMA is often interpreted as an Andean-type, subduction-related volcanic arc (Berberian & King, 1981), with volcanic and plutonic rocks ranging in age from upper Jurassic to Cenozoic. The peak volcanic activity is estimated to be of Eocene age (Berberian & King, 1981; Alavi, 1994).

Previous geophysical data on the lithospheric structure

No deep seismic sounding data are available in Iran besides shallow seismic reflection profiles for oil exploration. Bouguer anomalies have been used to estimate crustal thickness (Dehghani & Makris, 1984; Snyder & Barazangi, 1986) and, combined with geoid and topography, lithospheric thickness (Molinario et al., 2005). Recent receiver function analysis by Paul et al. (2006) shows

however that crustal thickness is strongly decorrelated with Bouguer anomalies. Based on the same field experiment as in this study, Paul et al. (2006) (hereafter referred to as PA06) estimate crustal thickness to be ~45 km between the Persian Gulf coast and the High Zagros after which it thickens rapidly to ~70 km within a narrow zone beneath the SSZ, before thinning to ~42 km beneath the UDMA and the southern rim of Central Iran. They propose that the localized thickening results from the overthrusting of the crust of Central Iran onto the Zagros crust along the MZT.

Studies of Pn velocities show high velocities in the Arabia plate including the Zagros (8.1-8.4 km.s⁻¹; Al-Lazki et al., 2004) and normal velocities (7.9-8.1 km.s⁻¹) beneath most of the Iranian plateau (Hearn and Ni, 1994; Al-Lazki et al., 2004). The transition from high to normal velocities occurs at the MZT in the Northwestern Zagros (Al-Lazki et al., 2004), and is interpreted as an indication for absent or very limited underthrusting of Arabia. In the southern Zagros the situation may be different as the high-velocity area seems to extend 100 km north of the MZT, but their resolution in that area is too poor to draw any firm conclusions. Sn waves are strongly attenuated in the Iranian Plateau (Sandvol et al., 2001), but this attenuation is not compatible with thin, hot lithosphere as the Pn velocities are normal. Due to limited resolution, the Sn blockage is possibly limited to an area of low Pn velocities in Northwestern Iran (Al-Lazki et al., 2004).

There is still some uncertainty as to the evolution of the oceanic slab which once subducted before continental collision. Maggi et al. (2000) showed from waveform modeling that there is no unequivocal evidence for mantle seismicity in the Zagros or north of it, and that the deep events all belong to the Makran subduction zone.

P -wave velocities in the mantle change across the area of the MZT, with velocities being a few percent higher beneath Arabia and Zagros than beneath Central Iran (Bijwaard et al., 1998; Piromallo & Morelli, 2003). S -wave velocities have mainly been obtained by large-scale surface wave analysis with a spatial resolution of several hundreds of kilometers (e.g. Curtis et al., 1998; Villaseñor et al., 2001; Maggi & Priestley, 2005) or limited to the crust and uppermost mantle (Rodgers et al., 1999). The best resolution in the top 200 km over the whole of Iran is probably obtained by Maggi & Priestley (2005) who show relatively low velocities down to 150 km beneath the Alborz, the Iranian plateau and the Zagros, whereas the South Caspian Sea and the Persian Gulf are underlain by fast mantle. They explained this velocity contrast by a thin lithosphere overlying an above-solidus temperature mantle beneath the Turkish-Iranian plateau, which would be compatible with partial delamination of the lower lithosphere.

To improve our understanding of the mantle processes beneath the Zagros belt it is now necessary to improve the lateral resolution of the velocity models. This is the scope of the present study.

Data acquisition and processing

A passive seismic experiment was carried out between November 2000 and April 2001 along a profile from Bushehr on the coast of the Persian Gulf, across the Zagros belt, to Posht-e-Badam in the southwest of Central Iran (Fig. 1; Kaviani, 2004; PA06). It was co-organized by Iranian and French seismologists from IIEES, Tehran and LGIT, Grenoble. The profile was oriented N42E, almost perpendicularly to the structural strike of Zagros. The array included 66 stations equipped with digital continuously-recording Agecodagis data acquisition systems with GPS time base, and various types of three-component sensors with 1s to 120s cutoff period. The broadband stations were installed in three short-aperture arrays (two triangles in the Zagros and four stations in Central Iran, see Fig. 1) to enable measurement of the incidence azimuth of the surface waves and improve the two-station dispersion studies (Cotte et al., 2000; Pedersen, 2006).

This study proposes a joint interpretation of the results of two types of seismic data analysis with complementary advantages and disadvantages. Firstly, Rayleigh wave dispersion curves are inverted for shear wave velocity models in two short-aperture broadband arrays located in the ZFTB and across the MZT suture region. The lateral resolution of this surface-wave study is poor since average velocity models are computed for two arrays of ~130 and ~300 km aperture. However, it gives a reliable estimate of velocity variations with depth including error bars and, more importantly, provides absolute *S*-wave velocities that can be interpreted in terms of compositional or thermal changes with depth. Secondly, teleseismic *P*-wave relative traveltime residuals are inverted for *P*-wave velocity variations in a depth cross-section under the profile using the ACH method (Aki et al., 1977). It gives robust results with respect to noise in the data or initial model parametrization (Evans & Achauer, 1993), with a lateral resolution of the order of a few station spacings, that is 20 to 30 km in our case. But ACH also has a number of important drawbacks including the projection of velocity heterogeneities located outside the target volume (beneath the network) into it (Masson & Trampert, 1997), and the impossibility to estimate vertical velocity variations as the anomalies mapped at different depths refer to different and unknown average layer velocities (Lévêque & Masson, 1999).

Surface wave analysis: S-wave velocity structure

Data selection and pre-processing

The database for the surface wave study is composed of records of Rayleigh waves (vertical component) from teleseismic events. For this analysis we used only data from STS-2 (120-s cutoff period) and CMG-3ESP (90-s cutoff period) sensors for which we analysed 70 events with epicentral distances between 25 and 160°, magnitudes greater than 5.5, and good signal-to-noise ratios (see a location map of epicenters in Fig. 2). The seismograms were corrected for instrumental responses and subsequently frequency-time filtered (Levshin, 1989) based on multiple filter analysis (Dziewonski et al., 1969) to minimize contamination by noise, spectral holes, higher modes and multipathing. Records with sign of mixture between the fundamental mode Rayleigh wave and other waves were rejected.

Array analysis

There are two major difficulties in surface wave analysis. Firstly, the waves may be significantly deviated from the great-circle (e.g. Alsina & Snieder, 1996; Cotte et al., 2000), and secondly the phases may be perturbed by wave interaction, which can be formalised by non-plane wavefronts (Wielandt, 1993). The latter problem can be at least partly resolved by using seismic events from different epicentral areas (Pedersen, 2006), however this increases the problem with great-circle deviation as it is then necessary to increase the angle that one allows for between the station profile and the event-station great-circle. A possible compromise for these difficulties is to increase the allowed angle as suggested above, but performing a first-order, frequency dependent, correction for the great-circle deviation by array analysis (Baumont et al., 2002; Bourova et al., 2005). We have followed this procedure here. The array analysis consists of defining a small (3-5 stations) array around the target profile, and at each frequency search for the plane wave which best fits observed time-delays between pairs of stations. The frequency-azimuth thus obtained is subsequently used to correct the two-station dispersion curve.

To compare the lithospheric structure between the Arabia plate (beneath Zagros, SW of MZT) and the micro-blocks of Central Iran (NE of MZT), we separated the available broadband stations in two sub-arrays, array AB (stations A1-A2-A3, B1-B2-B3) in the Zagros and array BCD (stations B1-B2-B3, C2, D1-D2-D3) further north (see Fig. 3a). The phase velocity measurements between stations C and D were unstable due to small inter-station distances which is why we had to add stations B1-B2-B3 to the northern array. The location map of Figure 3a shows that the longest paths of sub-array BCD, which are ~290 km long, consists of 230 km within the surface exposure

of the Sanandaj-Sirjan metamorphic zone (SSZ) and the Urumieh-Dokhtar magmatic assemblage (UDMA), and 60 km within the Zagros fold-thrust belt (ZFTB).

The phase velocity dispersion curves of the Rayleigh waves were measured between the stations of each sub-array and the mean dispersion curves were calculated for arrays AB and BCD. These curves, which are plotted in Figure 3b, document a strong phase velocity contrast of ~4.5% between 40 and 80s period, with higher phase velocities for sub-array AB. This result is consistent with previous surface-wave tomographic studies in the Middle East which documented slower *S*-wave velocities at ~100 km depth beneath Central Iran than beneath the Arabian platform (Debayle et al., 2001; Shapiro & Ritzwoller, 2002; Maggi & Priestley, 2005), but our results show that this transition is located within our study area, and most likely beneath sub-array BCD, which means that it is likely to take place somewhere within the northern edge of the Arabian platform or at its contact with the Central Iranian lithosphere.

To estimate the contribution of the part of the wave paths between stations B and the surface exposure of the MZT, which definitely belongs to the Arabia plate, we added to our dataset records of stations equipped with CMG-40 (60s) sensors and located northeast of the MZT. The dispersion curves between the broadband stations C1, D1, D2, D3, and the CMG-40 stations M4, M5, M6, M7 and M8 (see locations in Fig. 3a) were measured in the period range 20 to 60s. The resulting dispersion curve, which is indicative of the crust and uppermost mantle north of the MZT, is displayed as the thin black line with plain error bars in Figure 3b. It is almost identical to the dispersion curve measured for array BCD (thick plain black line) between 20 and 60s. We conclude that at least for this period range, dispersion measurements in array BCD are representative of the lithospheric structure northeast of the surface trace of the MZT.

***S*-wave velocity structure**

To obtain the *S*-wave velocity models in the lithosphere beneath sub-arrays AB and BCD, we applied the two-step Monte-Carlo inversion technique described in Bourova et al. (2005), which is a modification of the method of Shapiro et al. (1997). In the first step, a linearized inversion of the dispersion curve is carried out using the software of Herrmann (1987) to obtain a reasonable layered starting model. Then, a stochastic Monte-Carlo inversion is conducted, with the output model of the linearized inversion as starting model. In the crust, the model is parameterized by the thickness and constant velocity of each layer. To take into account the continuous velocity variation in the mantle, we consider that the mantle of the starting model consists of a few layers with a

constant velocity gradient in each layer and no velocity jumps are allowed across layer interfaces. There is only one more parameter to invert for as compared to a model with constant velocity layers. At each iteration of the Monte-Carlo inversion, random changes within given limits are applied to all model parameters. If the calculated dispersion curve falls within the error bars of the observations, the new model is accepted and used as the initial model for the next iteration. In the opposite case, the model is rejected and the next iteration starts from the last accepted model. To be certain of exploring most of the parameter space, we run the Monte Carlo inversion several times, with different random series of parameters.

As the starting model of the linearized inversion, we used a preliminary average *S*-wave velocity calculated by Maggi & Priestley (2005) for the Turkish-Iranian plateau. Even though the initial model (shown as a red dotted curve in Figure 4) is different from the final average model (MP05) published by Maggi & Priestley (2005), it is a better starting model because it contains no developed LVZ. Moho depth in the starting model was modified accordingly to the result of the receiver function analysis by PA06. The mean Moho depths beneath arrays AB and BCD were considered to be 45 and 55 km respectively. The crust was divided into 2 layers under sub-array AB. Beneath sub-array BCD, we added a third layer in the deepest 10 km of the crust to account for possible high velocities in the thickened lower crust of the SSZ, as suggested by the gravity models of PA06. In the subsequent Monte-Carlo inversion, we applied 1% random perturbations to *S*-wave velocities and 5% random perturbations to interface depths at each iteration. In total, 10000 models were tested, with 100 series of random parameters, and 100 iterations for each series.

The results of the inversion are presented in Figure 4. All models accepted in the inversion of dispersion curves of array AB are plotted in light blue, and models for array BCD in light red. The mean *S*-wave velocity models calculated for the two arrays are plotted as a thick blue line for AB, and a thick red line for BCD. Crustal velocities to 25-35 km depth are not constrained due to the lack of reliable dispersion measurements at periods shorter than 20s. In the upper mantle, the difference in the dispersion curves measured at AB and BCD in the 40-80s period range (Fig. 3b) results in a clear and well-resolved difference between the two sets of accepted *S*-wave velocity models in the depth range 50 to 170 km. The mean *S*-wave velocity structure beneath the Zagros (array AB) displays a gentle increase from $\sim 4.5 \text{ km.s}^{-1}$ at Moho depth (45 km) to $\sim 4.9 \text{ km.s}^{-1}$ at 250 km depth, below which the resolution decreases strongly. No low-velocity zone (LVZ) is detected in the resolved depth range beneath Zagros. For sub-array BCD, the minimum velocity of the average model is 4.4 km.s^{-1} at 80 km depth. The *S*-wave velocity increases again with depth

between 80 and 170 km depth where it converges with the velocity model measured at array AB (Fig. 4a). The decrease in velocity immediately beneath Moho is not well resolved due to trade-off with the lower crustal velocities.

Teleseismic traveltimes inversion: *P*-wave velocity structure

Traveltimes residuals

We investigated the *P*-wave velocity variations under the array by inverting teleseismic traveltimes residuals. Arrival times of *P* waves were picked on the records of 111 earthquakes with epicentral distances between 25° and 95° after correction for sensor response and subsequent bandpass filtering. The event hypocenters are shown in Figure 2. Only *P*-wave arrival times of events with 10 or more reliable readings were kept. The average number of readings per event is 46. Traveltimes residuals were calculated with respect to the IASP91 standard earth model (Kennett and Engdahl, 1991), and the average for each event was subtracted from the relevant residuals. This correction yields relative residuals that are presumably sensitive only to the velocity anomalies beneath the stations. The final dataset includes 5073 residuals at 66 stations.

Figure 5b shows the relative residuals along a N42 profile centered at [30.6°N,50.3°E], where $x=0$ corresponds to the MZT. The time residuals observed at a given station are averaged over all available events, and the resulting mean residual and its error bar are plotted at the abscissa of the station projected onto the N42 profile. The variations of the residuals with the back-azimuth are not well-resolved due to the concentration of 48% of the back-azimuths in the 70-120° range (see Fig. 2). Moreover, the quasi-linearity of our array combines with this incomplete azimuth coverage to prevent from inverting the residuals for 3-D structure. The orientation of the profile perpendicular to the structural trend of Zagros reduces the probability that 3-D heterogeneities in the vicinity of the 2-D profile have a strong influence on the residuals. To reduce this bias even more, we could use earthquakes whose back-azimuths differ by less than 30° from the average strike of the array, as done for example by Tilmann et al. (2003). However, this would leave only 26 events out of 111 and make the inversion meaningless.

The overall trend is that the residuals are negative (minimum -0.6s) at stations located in the Simple Folded Belt (SFB) of Southern Zagros and positive (maximum 0.5s) at stations in Central Iran. Apart from this long wavelength variation, the most significant lateral changes are the rapid increase at stations close to the MZT followed by a decrease to negative residuals in the SSZ, the increase from -0.5s to null residuals between the SFB ($x=-200$ km) and the High Zagros ($x=-100$

km), and the small and spatially limited decrease at ~175km. The difference between the most negative (at the NE end of the profile) and the most positive residual (close to the MZT) is 1.2 s.

The application of crustal corrections to teleseismic traveltimes before inversion using a priori information is an efficient method to attenuate smearing of crustal anomalies and increase the resolution in the mantle (e.g. Lippitsch et al., 2003; Martin et al., 2005). However, it requires a precise 3-D crustal velocity model constructed from reflection and refraction seismic data that is not available in our study region. A correction for crustal thickness variations using the Moho depth profile by PA06 and normal velocities ($\sim 6.7 \text{ km.s}^{-1}$) for the lower crust would strongly enhance the negative residuals in the SSZ. Based on gravity observations, it is however likely that the crustal velocities are anomalous in this area. We therefore chose not to apply crustal corrections in this study.

Inversion of residuals

We used the ACH damped-least-squares inversion method of Aki et al. (1977) to backproject the relative residuals and estimate the size and amplitude of *P*-wave velocity perturbations beneath the array. A comprehensive description of the method is given in Evans & Achauer (1993). More sophisticated iterative non-linear inversion schemes are available (e.g. Sandoval et al., 2004), but ACH is efficient enough to image the most significant velocity variations of interest to lithospheric exploration.

We tested the influence of block widths, layer thicknesses, and damping values, which are critical parameters for ACH inversion. The optimum parameters of the block model are given in Table 1. A damping value of 80 was selected from the trade-off curve between residual and model variances. The first layer of 10 km thickness includes cones to account for the static station corrections. To attenuate the influence of the horizontal sampling in discrete blocks, the final models were smoothed horizontally using the “shift-and-average” procedure of Evans & Achauer (1993).

The results of the ACH inversion of traveltime relative residuals are shown in Figure 5. Figure 5c displays velocity perturbations on a depth cross-section along the N42 profile. Two indicators of the resolution of the cross-section of Fig. 5c are displayed in Fig. 5d (number of ray hits per block) and 5e (diagonal element of the resolution matrix). This final velocity perturbation model explains 85% of the initial data variance. Figures 5d and 5e and results of synthetic tests indicate that the model is not well resolved in the crust (top 50 km, see Fig. 5d and 5e) and at depths greater than 250 km. The hit-count cross-section (Fig. 5d) shows that the number of rays per block is larger than

60 in most mantle blocks with two peaks above 150 hits at depth of 50 to 150 km beneath the two sets of stations that worked best during the experiment. The diagonal elements of the resolution matrix (Fig. 5e) are very low in many blocks of the crustal layer, due to weak ray crisscrossing. As mentioned in the introduction, the use of relative residuals implies that anomalies are computed with respect to an unknown velocity model (Lévêque & Masson, 1999). Thus, it is impossible to compare velocity anomalies at different depths, and we will only discuss lateral velocity variations. The most significant large-scale feature of the depth cross-section is the contrast in the uppermost mantle between the higher *P*-wave velocities beneath the Zagros and the lower velocities beneath the UDMA and the southern rim of the CIMC. The maximum change in velocity perturbation between the SW and NE ends of the profile is ~5% in the top mantle layer (50 to 100 km depth) and ~4% in the 100-150 km layer. At a smaller length scale, the positive and slightly negative residuals at stations in the MZT and SSZ regions (Fig. 5b) project into a negative and positive velocity anomaly in the two shallowest layers. The increase of residual in the High Zagros (between $x=-150$ km and $x=50$ km) gives a negative velocity anomaly in the crustal layer. Thus, the *P*-wave tomogram displays strong anomalies both at crustal and mantle depth.

Discussion

A strong lateral change in the upper mantle velocity structure

The Rayleigh wave dispersion study shows that the phase velocity at 40 to 80s period is significantly higher for paths in sub-array AB than for paths in sub-array BCD (Fig. 3b). Moreover, the similarity between the dispersion curves measured for BCD and the ones measured at stations located northeast of the MZT shows that, in the period range 20-60s, dispersion measurements in BCD are representative of the mantle structure northeast of the MZT (Fig. 3). At longer periods, we have no separate estimate of the dispersion for stations on the northeastern side of the MZT, and a *S*-wave velocity difference between the Zagros and the CIMC at depths larger than 150-170 km cannot be ruled out. However, we consider it as very unlikely because such a difference would lead to different phase velocities at stations of the northern side of the MZT and at BCD even at 60s.

The maximum difference between the mean phase velocities is 4.5% at 75s period. Furthermore, the teleseismic traveltimes study shows that the ~1.1s difference between the two ends of the profile (Fig. 5b) is projected by the ACH inversion into the crust and the uppermost mantle to a depth of 150-200 km, with higher velocities in the southwest than in the northeast (Fig. 5c). Therefore we have two independent arguments for a strong lateral change in seismic velocities in the upper mantle beneath our profile, with relatively higher *P* and *S* wave velocities beneath the Zagros

(Arabia plate) and lower velocities beneath UDMA and the southern rim of the CIMC (Iran micro-blocks). Both the surface wave analysis and the teleseismic travelttime inversion indicate that the velocity difference is likely to be limited to the uppermost mantle above 150 to 170 km.

The inversion of surface-wave dispersion curves provides absolute shear wave velocity models that can give clues on the mineralogical composition and/or the thermal state of the mantle. However, it is difficult to predict mineralogy and temperature in the continental lithosphere from shear velocities alone. We therefore limit our analysis to the comparison with reference global or regional *S*-wave velocity models. The surface-wave studies of the Arabian shield and platform by Rodgers et al. (1999) and Mokhtar et al. (2001) are restricted to the crust and the very shallow upper mantle (45s and 60s maximum period) so we focus the comparison (see Figure 4) on the standard earth model AK135 (Kennett et al., 1995) and the mean model for the Turkish-Iranian plateau measured by Maggi & Priestley (2005), referred to as model MP05 in the following. We also compare with a model estimated for the Proterozoic Baltic shield of Finland by Bruneton et al. (2004) because it corresponds to an unperturbed mantle shield structure with a typical shield geotherm and depleted composition as estimated by a large number of seismic stations.

The upper mantle *S*-wave velocities estimated for the Zagros region are between 0.1 and 0.6 km.s⁻¹ higher than in AK135 in the depth range 70-200 km, in agreement with the smooth shear wave velocity model of Shapiro & Ritzwoller (2002) and high *Pn* velocities beneath the Arabian platform including the Zagros (Al-Lazki et al., 2004). The comparison with MP05 also confirms that the mantle beneath the Zagros is faster than beneath the Turkish-Iranian plateau. Its lower error bound is close to the unperturbed Proterozoic of the Baltic shield. All this indicates that the mantle beneath Zagros has a shield-type structure. It is disputed whether a continental lithosphere-asthenosphere boundary, defined as the depth at which convection replaces conduction in heat transport, would be related to a LVZ (Poupinet et al., 2003; Priestley & McKenzie, 2006), but the consistently high velocities beneath sub-array AB point towards a lithosphere at least 250 km thick. To strengthen this assertion, we used the empirical relation for $V_s(P,T)$ (*S*-wave velocity as a function of pressure and temperature) derived by Priestley & McKenzie (2006) to estimate the temperature depth profile beneath AB from the average velocity profile of Figure 4. The temperature rises smoothly with depth between 100 and 250 km, without any rapid decrease in the temperature gradient which would mark the base of the lithosphere (Priestley & McKenzie, 2006). The low velocity zone immediately below the Moho in the mean model of sub-array BCD is less than 50 km thick. It is not well resolved as it is located at the very top of the mantle where the

trade-off between the crust and the mantle is significant. Moreover, velocities beneath BCD are higher than MP05 at most mantle depths and even higher than AK135 at depths greater than 130 km. Based on these observations, we believe that mantle lid delamination, as proposed by Maggi & Priestley (2005) and Molinaro et al. (2005), is unlikely for our study region.

Even though the hydration of mantle material can lower velocities significantly (e.g. Bruneton et al., 2004), the velocity contrast of almost 0.5 km s^{-1} between the two profiles is probably too strong to be created by compositional changes only (Sobolev et al., 1997; Goes et al., 2000), and we support the idea that the uppermost mantle temperatures on average are higher beneath sub-array BCD than beneath sub-array AB.

The result that the mantle beneath AB has a shield-like structure qualitatively agrees with the V_P tomogram of Fig. 5c. However, the 9% V_S contrast between AB and BCD at 80 km depth is stronger than the P -wave velocity lateral variation. According to the V_P tomogram, BCD is located right on the transition between the high-velocity upper mantle of the Arabian platform and the lower-velocity upper mantle of Central Iran (Fig. 5c). In the following, we assume that this boundary is the suture between the two lithospheres, and we further test the influence of its location on both the dispersion curves and P -wave tomography to try to reconcile the two observations.

Location of the suture in the upper mantle

The analysis of receiver functions by PA06 documents a strong increase in crustal thickness beneath the SSZ (see Moho depth profile in Fig. 5c). Their modeling of the Bouguer anomaly shows that this crustal thickening has to be compensated by thicker high-density material northeast of the MZT as compared to the area southwest of the MZT. These two elements suggest a crustal origin for at least part of the low and high velocity anomalies in the shallowest two layers of the V_P tomogram beneath the MZT and the SSZ. Such crustal anomalies would leak to mantle depth in the inversion due to weak ray crisscrossing in the crustal layer, and they would blur the image of the mantle in the suture region.

Yet we can combine the different types of information available and test different lithospheric models by forward modeling, that is by comparing observed residuals with those predicted for the models. The synthetic datasets are computed using the same ray tracing scheme as in the inversion (Evans & Achauer, 1993), for the same event-station couples, and they are inverted using the same parameters (block model, damping parameter) as for the actual dataset. In all the models we use the three-layer crustal geometry proposed by PA06. The second geometrical constraint is that we

assume the boundary between relatively fast and slow mantle velocities is a first-order vertical discontinuity. Numerical tests showed that more complex geometries or a gradual velocity change are possible but that they cannot be resolved by our data. We chose the maximum depth of the mantle V_P anomaly (150 km) in agreement with the S -wave average velocity profiles of Fig. 4 and the P -wave velocity tomogram of Fig. 5c. The next choice concerns the velocity contrast in the mantle lid. The V_S and V_P inversions indicate that the long wavelength traveltime variation is due to a lateral change in the mantle velocity. Considering the thickness of the heterogeneous mantle layer, a V_P change of 6% is required (+3% beneath the ZFTB and -3% beneath the UDMA and CIMC) to fit the difference in traveltime residual between stations located at $x < -200$ km and $x > 200$ km.

Figure 6a shows the observed and predicted residuals with a mantle boundary 135 km north of the MZT and normal crustal velocities (4.7 km.s^{-1} for the sediments, 5.8 km.s^{-1} for the upper crust, and 6.5 km.s^{-1} for the lower crust; model A) as proposed by Hatzfeld et al. (2003) from the inversion of arrival times of microearthquakes and receiver functions in the Ghir region. The geometry of the crustal layers induces apparent lateral velocity variations in the 50-km thick crustal block layer as shown in Fig. 6b. The mantle velocity contrast cannot be moved more further north and still fit the observed dispersion curves within their error bars. The predicted residuals fit the long-wavelength variation however the short-wavelength variations immediately north of the MZT ($x=0$ to 200 km) are not explained by this model. We explored a large number of mantle velocity models but there is no way of adequately explaining the short-wavelength variations north of the MZT without increasing the velocity in the lower crustal layer (6.7 km.s^{-1}) and decreasing the velocity in the sediments (4.5 km.s^{-1}) and upper crustal layer (5 km.s^{-1}) (model B, Figure 7). This corresponds in practice to increasing the lateral velocity variations in the crustal block layer, as shown by Figure 7b. In this case, the short-wavelength residuals are fitted adequately (Fig. 7a). The velocity in the crystalline upper crust in model B is unrealistically low, but it is imposed by the geometry of the crustal model in which the positive residuals in the MZT region are explained by a thickening of the upper crustal layer. A more reliable hypothesis is that the late P arrivals observed at stations close to the MZT are partly due to a thickening of the sediments in the accretionary wedge in front of the thrust.

The inversion of the synthetic residuals gives a tomogram (Fig. 7c) which is very similar to the result of the inversion of the observed dataset (Fig. 5c). This inversion shows that the crustal structure necessary to fit the short-wavelength residual variations blurs the image of the mantle

below. In spite of the blurred mantle image, it is not possible to push the vertical mantle boundary significantly towards the southwest without introducing unrealistic velocities in the crust. For example, a model with no velocity perturbation (0%) in the 50-100-km layer between the MZT and the vertical boundary of Figures 6 and 7 gives a correct fit to the residual curve only with a very high velocity in the crustal root ($V_p=7.5 \text{ km.s}^{-1}$) and an unrealistically high velocity of 6.9 km.s^{-1} in the lower crustal layer outside the crustal root. Such high velocities (and the associated densities) are difficult to reconcile with the rather strong *P*-to-*S* conversions at the Moho observed by PA06 and with the observed Bouguer anomaly.

The boundary between the two lithospheric mantles is probably not a vertical first order discontinuity as in Figure 7b. We tested different other geometries, including a dipping suture and a smooth velocity transition rather than an abrupt change. However, the image resulting from the inversion is always blurred by the crustal velocity anomalies and no complementary information can be deduced from the V_p tomography.

Similarly, we have introduced the Tethyan oceanic lithosphere (modeled as 100-km thick slab with 2% higher V_p than the surrounding mantle and a 45° dip toward the northeast) still attached to the Arabian margin in our synthetic models to test whether it was detectable or not. These tests show that due to smearing of the high-velocity crustal SSZ anomaly and the poor resolution at depths larger than 250 to 300 km, the question of the Tethyan slab being attached to the Arabian margin or detached from it cannot be answered by the ACH tomography.

Conclusions

This first high-resolution study of the lithospheric structure across the Zagros belt documents a strong lateral change of both *P* and *S* wave velocities in the shallow mantle beneath the profile. The dispersion curves of the Rayleigh fundamental mode measured in two short-aperture arrays located on each side of the MZT display clear differences. In the Zagros, the average shear wave velocity model deduced from the dispersion curve is characterized by high velocities from $4.5\pm 0.2 \text{ km.s}^{-1}$ below the Moho ($\sim 45 \text{ km}$) to $4.9\pm 0.25 \text{ km.s}^{-1}$ at 200 km depth. The second short-aperture array (BCD) which covers the MZT region, the SSZ, the UDMA and the southern rim of the CIMC gives lower *S*-wave velocities in the mantle from the Moho to 150 km depth where both models converge to $\sim 4.9 \text{ km.s}^{-1}$. This average velocity model includes a rather thin ($< 50 \text{ km}$) and poorly-resolved LVZ with a minimum of $4.4\pm 0.2 \text{ km.s}^{-1}$ at 80 km depth. The comparison of these shear wave velocity models with the standard earth model AK135, a model calculated for a Proterozoic part of the Baltic shield, and with the results of previous studies conducted in our study region (Al-Lazki et

al., 2004; Maggi & Priestley, 2005) indicates that the mantle of the Arabian platform beneath Zagros has a shield-like *S*-wave velocity structure. The 0.5 km.s^{-1} difference between the two V_s models in the shallow mantle is likely due to a compositional change (presence of hydrated minerals for example) associated with higher temperatures beneath the MZT, the SSZ and the UDMA than beneath the Zagros. However, we believe that the absolute *S*-wave velocities measured in array BCD are too high to support the hypothesis of mantle lid delamination in this transition zone between Arabia and Central Iran. Teleseismic *P* wave arrivals are 1.1s earlier at stations in the Simple Folded Belt than in Central Iran, confirming the *S* velocity variation inferred from the dispersion measurements. Assuming that the time-shift is only due to mantle heterogeneity, it can be explained by a ~6% difference of *P*-wave velocity in a 105-km thick laterally heterogeneous shallow mantle. The backprojection of traveltimes to *P* wave velocity anomalies at depth gives a maximum velocity contrast of 4 to 5% in the two shallowest mantle layers (50-100 km; 100-150 km) between the Zagros and Central Iran. The tomogram also shows that array BCD, where we measured low phase velocities, is located right above the transition zone between the high-velocity mantle of the Arabian platform and the low-velocity upper mantle of Central Iran.

A striking result of the *P* traveltimes study is the heterogeneity of the crust in the middle part of the transect below the High Zagros, the MZT and the Sanandaj-Sirjan metamorphic zone. With respect to stations in the High Zagros, teleseismic *P* waves are ~0.5s earlier in the Simple Fold Belt, ~0.5s later in the MZT area, and ~0.2s earlier in the middle of the SSZ. The computation of synthetic traveltimes in lithospheric models assuming the crustal geometry proposed by Paul et al. (2006) shows that a correct fit to the observed residuals requires that the pronounced crustal thickening is compensated by an extension of the upper mantle Zagros high-velocity lid beneath the SSZ. The model of crustal overthrusting (Agard et al., 2005; Paul et al., 2006) explains at least qualitatively the short-wavelength anomalies of the relative residuals and the crustal velocity perturbations in the V_p tomogram of Figure 5c. The positive residuals in the MZT area and the associated low-velocity anomaly to 100 km depth could be created by the thickened crust and the thickened sediments of the accretionary wedge in the front wall of the MZT. The high-velocity anomaly beneath the SSZ would be due to the duplication of the lower crustal layer in the crustal-scale thrust in combination with high velocities in the shallow mantle to compensate for low velocities related to crustal thickening.

The inversion of P traveltime residuals is poorly resolved in the crustal layer due to weak ray criss-crossing. Moreover, the thickened crust induces a negative velocity perturbation in the shallowest mantle layer (50-100 km). As a result, the crustal heterogeneities leak to mantle layers and blur the tomogram, in particular in the region of the suture between the two lithospheric blocks. The location of the boundary between the high- and low-velocity regions of the upper mantle can only be estimated by trial-and-error fitting of the residual curve and the tomogram using synthetic models of V_p variations. The main argument for a boundary beneath the northern border of the SSZ is that a crustal anomaly alone cannot explain the early residuals observed in the SSZ. A model with a boundary located 135 km northeast of the MZT also gives Rayleigh wave phase velocities within the error bars of the dispersion measurements for array BCD. The exact shape of the boundary remains unknown due to the smearing of crustal anomalies.

As most events used in the ACH tomography have back-azimuths concentrated in the eastern quadrant (70-120°) not far from the strike of the Tethyan oceanic lithosphere (~40°) if it was still attached to the Arabian margin, the influence of the associated high-velocity slab on P -wave residuals would combine with the effect of crustal and upper mantle heterogeneity in the suture region, making it impossible for the ACH inversion to discriminate between the 3 anomalies. This is the reason why the V_p tomogram gives no definite answer on the presence or the absence of the Tethyan slab attached to the margin. However, other elements including the lack of high shear wave velocities at depths greater than 150 km beneath BCD array (Fig. 4) and the absence of any clear P -to- S conversion beneath the Moho at the northern end of the receiver function profile (Paul et al., 2006), suggest that the slab could be detached.

In Figure 8 we present a schematic model of lithospheric structure across Central Zagros. This model assumes that the boundary between the high- and low-velocity upper mantle lids coincides with the suture between the passive margin of the Arabian platform and the Tethyan oceanic mantle, or the upper mantle of the micro-blocks of Central Iran if the slab is detached. The lithosphere-asthenosphere boundary is plotted as a dotted line because we could not constrain its depth or its geometry. This hypothesis agrees with the model of crustal-scale thrust proposed by Agard et al. (2005) on geological arguments and by Paul et al. (2006) on geophysical arguments. The model implies that the upper mantle of the Arabian lithosphere extends to ~120 km northeast of the surface trace of the MZT assuming there is no decollement at the Moho.

Acknowledgments: The Zagros 2000-2001 experiment was funded by IIEES Tehran (Iran) and INSU-CNRS (France, programme IT). AK received a grant from the French Embassy in Tehran for his Ph-D thesis. Seismic stations used in this experiment belonged to the French national pools Lithoscope and RLBM of INSU-CNRS. We warmly thank all the people who participated in the field work, in particular the car drivers of IIEES. The dataset was preprocessed and assembled with the BDsis software developed by C. Péquegnat. We thank the reviewers for particularly insightful comments.

FIGURE CAPTIONS

Figure 1. Location map of the seismic array. a) Topographic map of Iran and neighboring regions. The small red triangles are the seismic stations used in this study. b) Tectonic map showing the main morphotectonic units of the study area and the stations. The thick dash-dot line is the N42 profile used to compute all cross-sections.

Figure 2. Epicenter map of earthquakes used in the surface-wave study (70 events plotted as red stars) and in the teleseismic tomography (111 events plotted as black and red stars). Azimuthal equidistant projection centered on [30.6°N, 53°E].

Figure 3. Results of Rayleigh wave dispersion measurements. a) Location map of the mini-arrays of broadband stations (plotted as red stars), and stations with CMG-40 sensors (red triangles) used in the dispersion measurements. The thick line segments show the locations of sub-array AB (in blue), BCD (in red), and MCD (stations M4, M5, M6, M7, M8, C2, D1, D2, D3; in black). b) Dispersion curves measured in sub-arrays AB (blue), BCD (red) and MCD (black).

Figure 4. Results of the inversion of Rayleigh wave dispersion curves for *S*-wave velocity models and comparison with other models. Accepted models are plotted as thin lines, in blue for sub-array AB and in red for sub-array BCD. The thick lines show the average models. The dotted red line is the starting model for the inversion. The standard earth model AK135, the model measured by Bruneton et al. (2004) for unperturbed Proterozoic mantle in the Baltic shield, and the average shear wave velocity model MP05 measured for the Turkish-Iranian plateau by Maggi & Priestley (2005) are plotted as black lines for comparison.

Figure 5. Observed *P*-wave relative teleseismic traveltimes residuals, and results of the ACH inversion for V_P perturbations. a) Average elevations along the N42 profile shown in Figure 1b. The grey triangles correspond to seismic stations. The three vertical lines show the boundaries of the main morphotectonic units. b) *P* traveltimes relative residuals plotted for each station at the abscissa of the projection of the station onto the N42 profile. c) Depth cross-section along the N42 profile in the 3-D model of *P*-wave velocity perturbations resulting from the inversion of residuals. The black solid line is the Moho depth profile measured by Paul et al. (2006) along

the same transect. The vertical dotted lines bound the areas covered by surface wave dispersion measurements in sub-arrays AB and BCD. d) Number of rays per block. e) Diagonal elements of the resolution matrix. ZFTB: Zagros Fold-Thrust Belt; MZT: Main Zagros Thrust; SSZ: Sanandaj-Sirjan metamorphic Zone; UDMA: Urumieh-Dokhtar Magmatic Assemblage; CIMC: Central Iran Micro-Continent; SFB: Simple Folded Belt; KZF: Kazerun Fault.

Figure 6. Synthetic model A. The crust has the three-layer structure proposed by Paul et al. (2006) with velocities 4.7 km.s^{-1} , 5.8 km.s^{-1} and 6.5 km.s^{-1} . The velocity perturbation is 3% in the upper mantle beneath the ZFTB, the MZT and the SSZ, and -3% beneath the UDMA and CIMC. a) Comparison between observed (empty squares with black error bars) and modeled (red dots) P traveltimes residuals. b). Synthetic lateral V_P perturbations averaged over depth in each layer of the ACH inversion (0-50 km, 50-100 km, 100-150 km). Note the strong negative anomaly (maximum: -5.9%) induced in the 50-100 km layer by the crustal thickening beneath the SSZ.

Figure 7. Synthetic model B with crustal layer velocities 4.5 km.s^{-1} , 5 km.s^{-1} , 6.7 km.s^{-1} . a) Comparison between observed and modeled P traveltimes residuals. Normally distributed noise with standard deviation of 0.2s has been added to the synthetic residuals before inversion. b). Depth-averaged synthetic lateral V_P perturbations. c) Depth cross-section in the model of V_P perturbations resulting from the inversion of synthetic residuals.

Figure 8. Proposed schematic interpretation of the lithospheric structure across Central Zagros. The Moho depth profile and the trace of the crustal-scale thrust that outcrops at the MZT and roots at Moho depth are from Paul et al. (2006). The results of the surface-wave dispersion analysis and teleseismic P traveltimes study are schematized as the green (high velocities) and pink (low velocities) areas in the mantle. The geometry proposed for the base of the lithosphere (dashed line) is speculative. The location of the boundary between the two lithospheres is marked by the hatched pattern. Its exact geometry remains unknown. The question mark on the dash-dot line indicates that we have no definitive element in favor or against the presence of the Tethyan slab attached to the margin of the Arabian platform.

References

- Agard, P., J. Omrani, L. Jolivet, and F. Mouthereau, 2005. Convergence history across Zagros (Iran): constraints from collisional and earlier deformation, *International Journal of Earth Sciences*, doi 10.1007/s00531-005-0481-4.
- Aki, K., A. Christoffersson, and E.S. Husebye, 1977. Determination of 3-dimensional seismic structure of the lithosphere, *J. Geophys. Res.*, 82(2), 277-296.
- Alavi, M., 1994. Tectonics of the Zagros orogenic belt of Iran: new data and interpretations, *Tectonophysics*, 229, 211-238.
- Al-Lazki, A.I., E. Sandvol, D. Seber, M. Barazangi, N. Türkelli, and R. Mohamad, 2004. Pn tomographic imaging of mantle lid velocity and anisotropy at the junction of the Arabian, Eurasian and African plates, *Geophys. J. Int.*, 158, 1024-1040.
- Alsina, D., and R. Snieder, 1996. Constraints on the velocity structure beneath the Tornquist-Teisseyre Zone from beam-forming analysis, *Geophys. J. Int.*, 126, 205-218.
- Baumont, D., A. Paul, G. Zandt, S.L. Beck, and H. Pedersen, 2002. Lithospheric structure of the central Andes based on surface wave dispersion, *J. Geophys. Res.*, 107 (B12), 2371, doi:10.1029/2001JB000345.
- Berberian, M., 1995. Master blind thrust faults hidden under the Zagros folds: active basement tectonics and surface morphotectonics, *Tectonophysics*, 241, 193-224.
- Berberian, M., and G.C.P. King, 1981. Towards a paleogeography and tectonic evolution of Iran, *Can. J. Earth Sci.*, 18, 210-65.
- Bijwaard, H, W. Spakman, and E. R. Engdahl, 1998. Closing the gap between regional and global travel time tomography, *J. Geophys. Res.*, 103, 30055-30078.
- Bird, P., 1978. Finite element modeling of lithosphere deformation: the Zagros collision orogeny, *Tectonophysics*, 50, 307-336.
- Bourova, E., H. Pedersen, T. Yanovskaya, and D. Hatzfeld, 2005. Surface-wave tomography in the Aegean region, *Geophys. J. Int.*, **160**,1006-1019.
- Bruneton, M., H.A. Pedersen, V. Farra et al., 2004. Complex lithospheric structure under the central Baltic Shield from surface wave tomography, *J. Geophys. Res.*, 109, B10303, doi:10.1029/2003JB002947.
- Cotte, N., Pedersen, H.A., Campillo, M., Farra, V., and Cansi, Y., 2000, Off-great-circle propagation of intermediate-period surface waves observed on a dense array in the French Alps. *Geophys. Jou. Int.*, 142(3), 825-840.
- Curtis, A., J. Trampert, R. Snieder, and B. Dost, 1998. Eurasian fundamental mode surface wave phase velocities and their relationship with tectonic structures, *J. Geophys. Res.*, 103 (B11), 26919-26947.
- Davoudzadeh, M., B. Lammerer, and K. Weber-Diefenbach, 1997. Paleogeography, stratigraphy, and tectonics of the tertiary of Iran, *N. Jb. Geol. Paläont. Abh.*, 205, 33-67.
- Debayle, E., J-J. Leveque, and M. Cara, Seismic evidence for a deeply rooted low-velocity anomaly in the upper mantle beneath the northeastern Afro-Arabian continent, *Earth Planet. Sci. Lett.*, 193 (3-4), 423-436.
- Dehghani, G. A., and J. Makris, 1984. The gravity field and crustal structure of Iran, *N. Jb. Geol. Palaeont. Abh.*, 168, 215-229.
- Dziewonski, A.M., S. Bloch, and N. Landisman, 1969. A technique for the analysis of transient seismic signals, *Bull. seism. Soc. Am.*, 59, 427-444.
- Evans, J.R., and U. Achauer, 1993. Teleseismic velocity tomography using the ACH method: theory and application to continental-scale studies, in: *Seismic tomography, Theory and practice*, H.M. Iyer and K. Irahara (eds), Chapman & Hall, London, pp. 319-360.

- Falcon, N. L., 1974. Southern Iran: Zagros mountains, *Spec. pub. Geol. Soc. London*, 4, 199-211.
- Goes, S., R. Govers, and P. Vacher, 2000. Shallow mantle temperatures under Europe from P and S wave tomography, *J. Geophys. Res.*, 105, doi:10.129/1999JB900300.
- Hatzfeld, D., M. Tatar, K. Priestley, and M. Ghafory-Ashtyany, 2003. Seismological constraints on the crustal structure beneath the Zagros mountain belt (Iran), *Geophys. J. Int.*, 155, 403-410.
- Hearn, T.M., and J.F. Ni, 1994. Pn velocities beneath continental collision zones: the Turkish-Iranian Plateau, *Geophys. J. Int.*, 117, 273-283.
- Herrmann, R.B., 1987. Computer programs in seismology, Vol. IV: Surface waves inversion, St Louis University, Missouri.
- Kaviani, A., 2004. La chaîne de collision continentale du Zagros (Iran): structure lithosphérique par analyse de données sismologiques, PhD thesis, Université Joseph Fourier, Grenoble.
- Kennett, B.L.N., and E.R. Engdahl, 1991. Traveltimes for global earthquake location and phase identification, *Geophys. J. Int.*, 105, 429-465.
- Kennett, B.L.N., E.R. Engdahl, and R. Buland, 1995. Constraints on seismic velocities in the Earth from travel-times, *Geophys. J. Int.*, 122, 108-124.
- Lévêque, J.-J., and F. Masson, 1999. From ACH tomography to absolute velocity models, *Geophys. J. Int.*, 137, 621-629.
- Levshin, A.L., 1989. Surface waves in media with weak lateral inhomogeneity, in *Seismic surface waves in laterally inhomogeneous Earth*, V.I. Keilis-Borok (ed.), Kluwer Academic Pubs, Dordrecht, pp. 35-69.
- Lippitsch, R., E. Kissling, and J. Ansorge, Upper mantle structure beneath the Alpine orogen from high-resolution teleseismic tomography, 2003. *J. Geophys. Res.*, 108, B8, 2376, doi:10.129/2002JB002016.
- Maggi, A., J. A. Jackson, K. Priestley, and C. Baker, 2000. A re-assessment of focal depth distributions in southern Iran, the Tien Shan and northern India: do earthquakes really occur in the continental mantle? *Geophys. J. Int.*, 143, 629-661.
- Maggi, A., and K. Priestley, 2005. Surface waveform tomography of the Turkish-Iranian plateau, *Geophys. J. Int.*, 160, 1068-1080.
- Martin, M. J.R.R. Ritter and Calixto Working Group, High-resolution teleseismic body-wave tomography beneath SE Romania - I. Implications for three-dimensional versus one-dimensional crustal correction strategies with a new crustal velocity model, *Geophys. J. Int.*, 162, 448-460.
- Masson, F., and J. Trampert, 1997. On ACH, or how reliable is regional teleseismic delay time tomography? *Phys. Earth Planet. Int.*, 102, 21-32.
- McQuarrie, N., J. M. Stock, C. Verdel, and B. P. Wernicke, 2003. Cenozoic evolution of Neotethys and implications for the causes of plate motions, *Geophys. Res. Lett.*, 30, 2036, doi: 10.1029/2003GL017992.
- Mokhtar, T.A., C.J. Ammon, R.B. Herrmann, and H.A.A. Ghalib, 2001. Surface wave velocities across Arabia, *Pure appl. geophys.* 158, 1425-1444.
- Molinaro, M., H. Zeyen, and X. Laurencin, 2005. Lithospheric structure beneath the south-eastern Zagros Mountains, Iran: recent slab break-off? *Terra Nova*, 17, 1-6.
- Paul, A., A. Kaviani, D. Hatzfeld, J. Vergne, and M. Mokhtari, 2006. Seismological evidence for crustal-scale thrusting in the Zagros mountain belt (Iran), *Geophys. J. Int.*, 166, 227-237.
- Pedersen, H.A., 2006. Impacts of non-plane waves on two-station measurements of phase velocities, *Geophys. J. Int.*, 165, 279-287.
- Piomallo, C., and Morelli, A., 2003, P wave tomography of the mantle under the Alpine-Mediterranean area, *J. Geophys. Res.*, **108**, doi:10.129/2002JB001757.

- Poupinet G., N. Arndt, and P. Vacher, 2003. Seismic tomography beneath stable tectonic regions and the origin and composition of the continental lithospheric mantle, *Earth planet. Sci. Lett.*, 212, 89-101.
- Priestley, K., and D. McKenzie, 2006. The thermal structure of the lithosphere from shear wave velocities, *Earth Planet. Sci. Lett.*, 244, 285-301.
- Regard, V., C. Facenna, J. Martinod, O. Bellier, and J. C. Thomas, 2003. From subduction to collision: Control of deep processes on the evolution of convergent plate boundary, *J. Geophys. Res.*, 108 (B4), 2208, doi:10.129/2002JB001943.
- Ricou, L. E., J. Braud, and J. H. Brunn, 1977. Le Zagros, *Mém. h. sér. Soc. Géol. Fr.*, 8, 33-52.
- Rodgers, A.J., W.R. Walter, R.J. Mellors, A.M.S. Al-Amri, and Y-S. Zhang, 1999. Lithospheric structure of the Arabian Shield and Platform from complete regional waveform modelling and surface wave group velocities, *Geophys. J. Int.*, 138, 871-878.
- Sandoval, S., E. Kissling, and J. Ansorge, 2004. High-resolution body wave tomography beneath the SVEKALAPKO array – II. Anomalous upper mantle structure beneath the central Baltic shield, *Geophys. J. Int.*, 157, 200-214.
- Sandvol, E., K. Al-Damegh, A. Calvert, D. Seber, M. Barazangi, R. Mohamad, R. Gök, N. Türkelli, and C. Gürbüz, 2001. Tomographic imaging of Lg and Sn propagation in the Middle East, *Pure appl. geophys.*, 158, 1121-1163.
- Shapiro, N.M., M. Campillo, A. Paul, S.K. Singh, D. Jongmans, F.J. Sanchez-Sesma, 1997. Surface-wave propagation across the Mexican Volcanic Belt and the origin of the long-period seismic-wave amplification in the Valley of Mexico, *Geophys. J. Int.*, 128, 151-166.
- Shapiro N.M., and M.H. Ritzwoller, Monte-Carlo inversion for a global shear-velocity model of the crust and upper mantle, *Geophys. J. Int.*, 151, 88-105.
- Snyder D. B., and M. Barazangi, 1986. Deep crustal structure and flexure of the Arabian plate beneath the Zagros collisional mountain belt as inferred from gravity observations, *Tectonics*, 5, 361-373.
- Sobolev, S.V., H. Zeyen, M. Granet, U. Achauer, C. Bauer, F. Werling, R. Altherr, and K. Fuchs, 1997. Upper mantle temperatures and lithosphere-asthenosphere system beneath the French Massif Central constrained by seismic, gravity, petrologic and thermal observations, *Tectonophysics*, 275, 1430164.
- Stöcklin, J., 1968. Structural history and tectonics of Iran: A review, *American Association of Petroleum Geologists Bulletin*, 52, 1229-1258.
- Stöcklin, J., 1974. Possible ancient continental margins in Iran, in *Geology of Continental Margins*, C. Burke & C. Drake eds., pp. 873-877, New York.
- Stoneley, R., 1981. The geology of the Kuh-e Dalneshin area of Southern Iran, and its bearing on the evolution of Southern Tethys, *J. Geol. Soc. London*, 138, 509-526.
- Tilmann, F., J. Ni, and INDEPTH III Seismic Team, 2003. Seismic imaging of the downwelling Indian lithosphere beneath Central Tibet, *Science*, 300, 1424-1427.
- Vernant, P., F. Nilforoushan, D. Hatzfeld, M. R Abassi, C. Vigny, F. Masson, H. Nankali, J. Martinod, A. Ashtiani, R. Bayer, F. Tavakoli, and J. Chéry, 2004. Present-day crustal deformation and plate kinematics in the Middle East constrained by GPS measurements in Iran and northern Oman, *Geophys. J. Int.*, 157, 381-398.
- Villaseñor A., M.H. Ritzwoller, A.L. Levshin, M.P. Barmin, E.R. Engdahl, W. Spakman, and J. Trampert, 2001. Shear velocity structure of central Eurasia from inversion of surface wave velocities, *Phys. Earth Planet. Int.*, 123 (2-4), 169-184.
- Wielandt, E., 1993. Propagation and structural interpretation of nonplane waves, *Geophys. J. Int.*, 113, 45-53.

Layer number	Thickness (km)	Block size (km)
1	10	Cones
2	40	20 x 20
3	50	30 x 30
4	50	40 x 40
5	50	40 x 40
6	60	50 x 50

Table 1. Parameters of the layered block model used in the inversion of teleseismic *P* residuals.

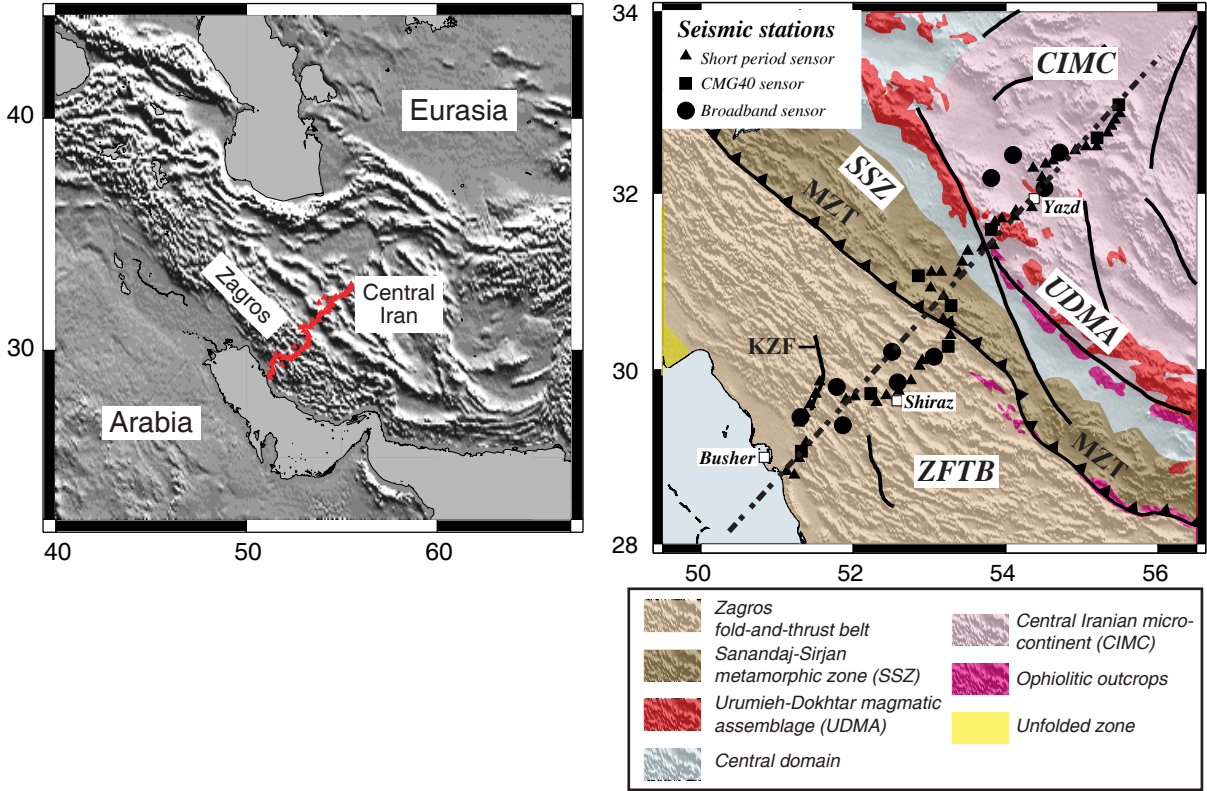


Figure 1

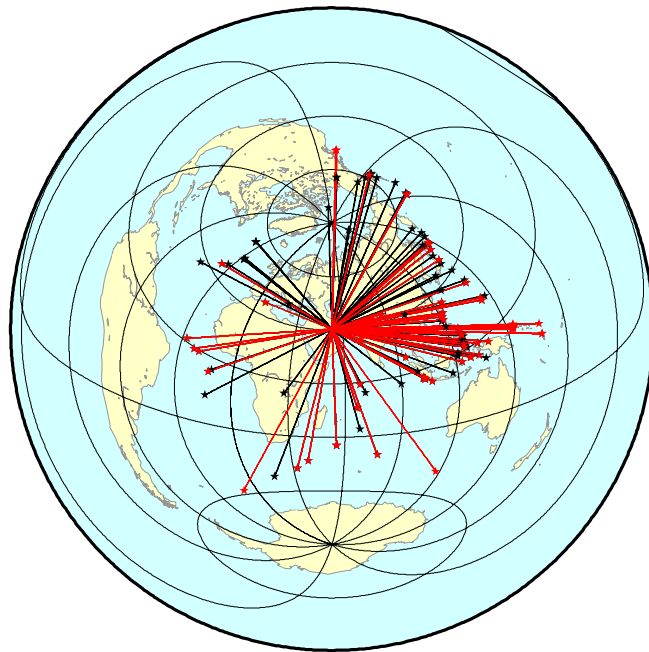


Figure 2

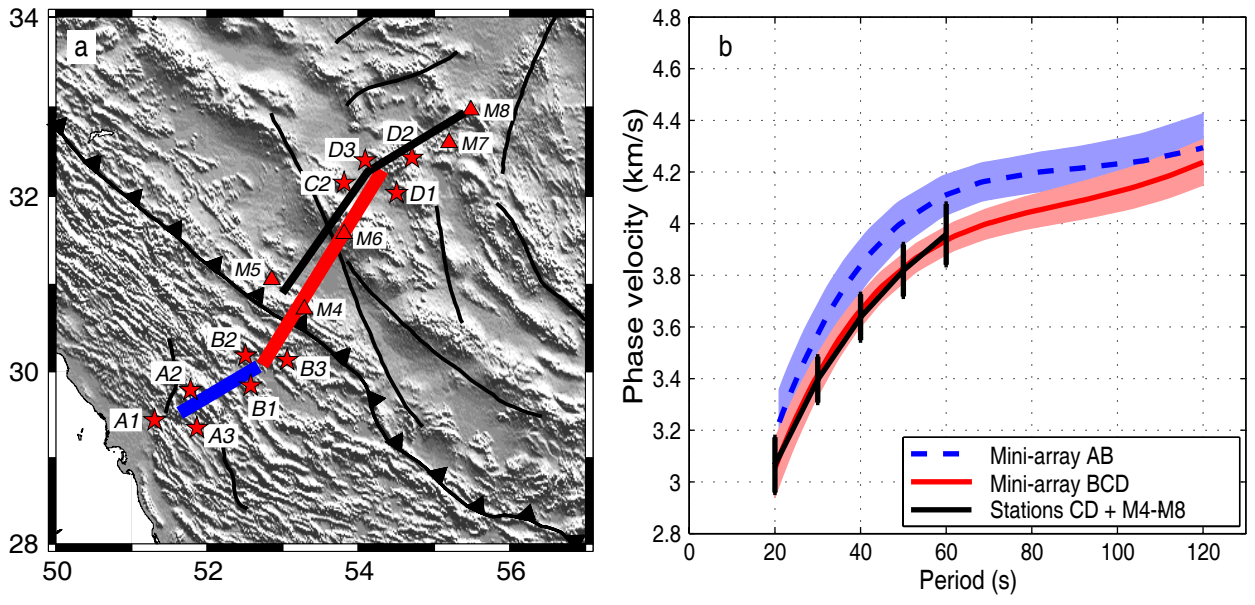


Figure 3

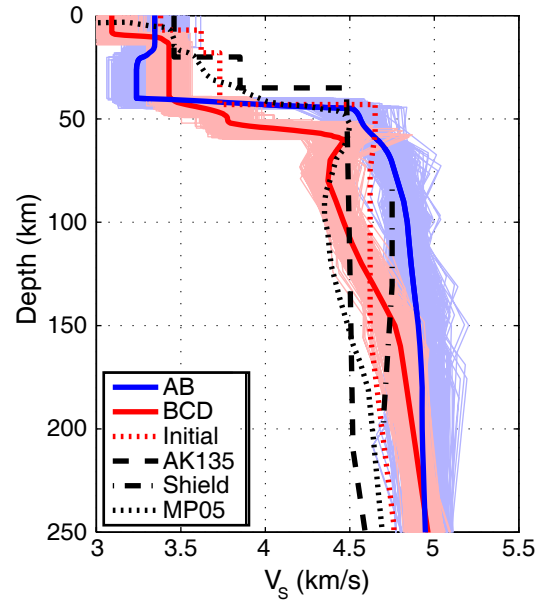


Figure 4

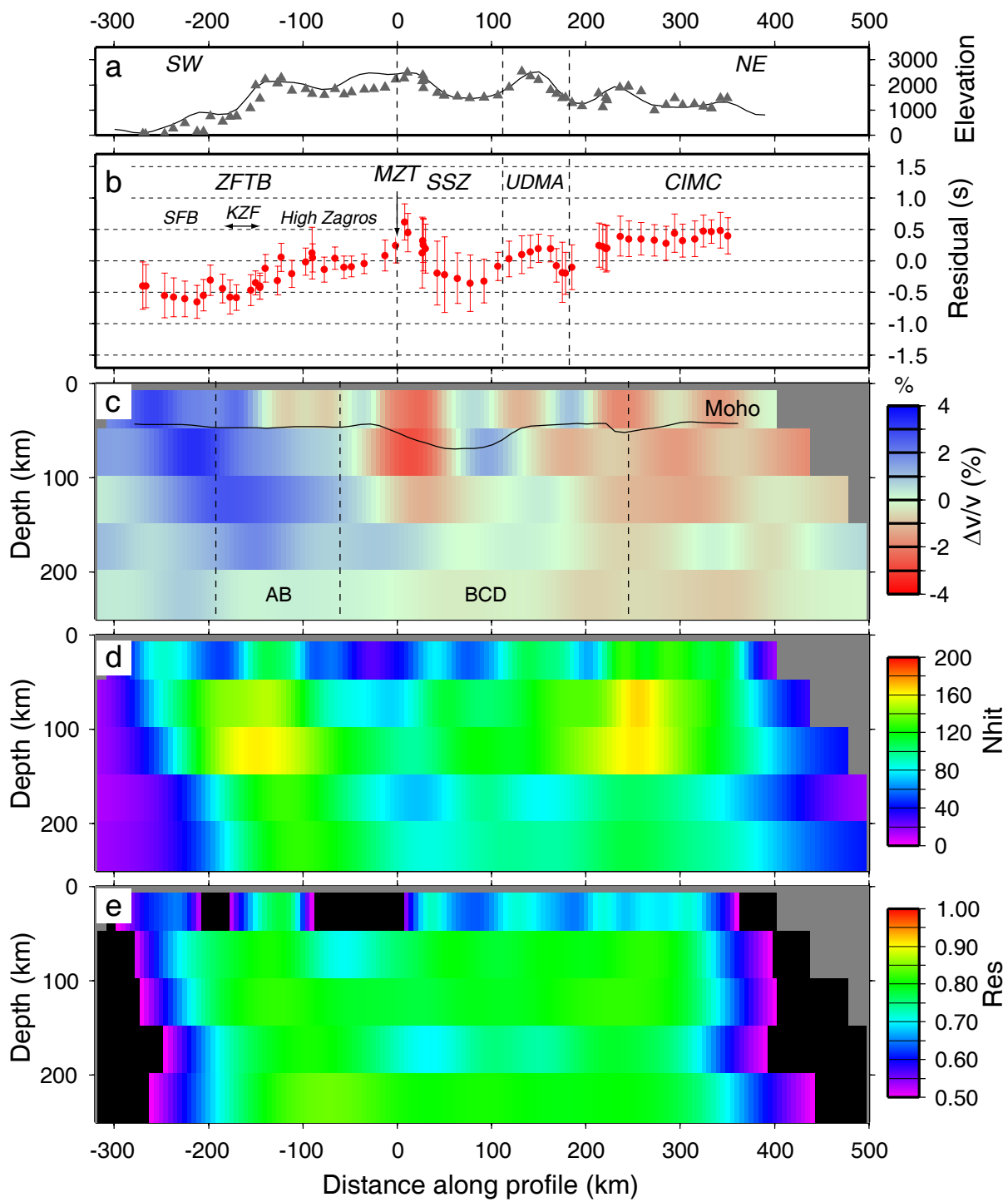


Figure 5

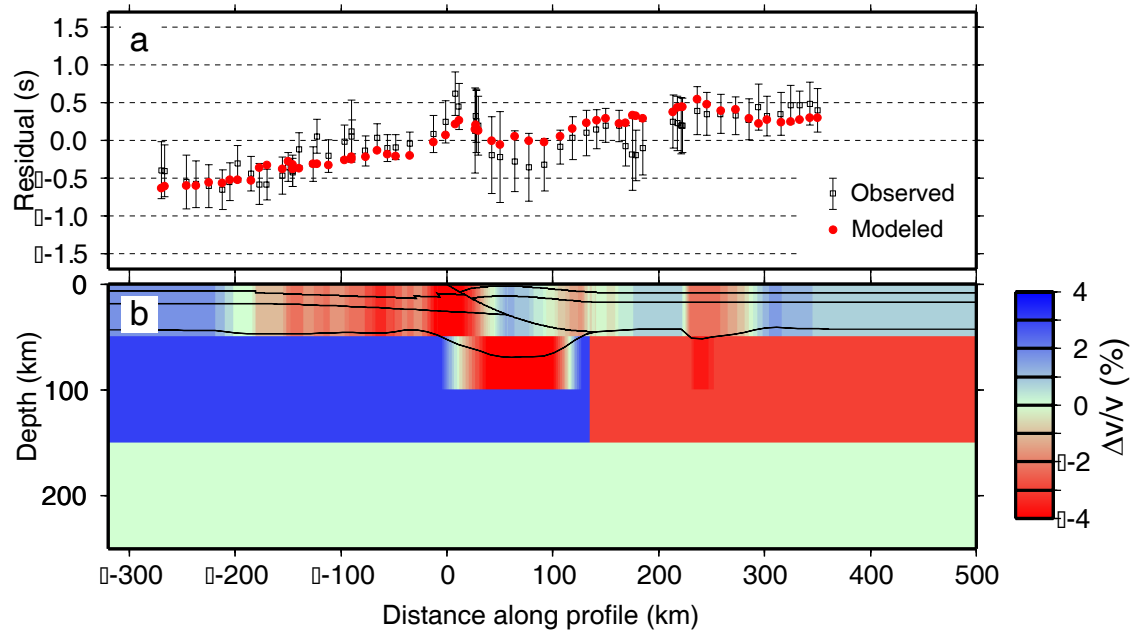


Figure 6

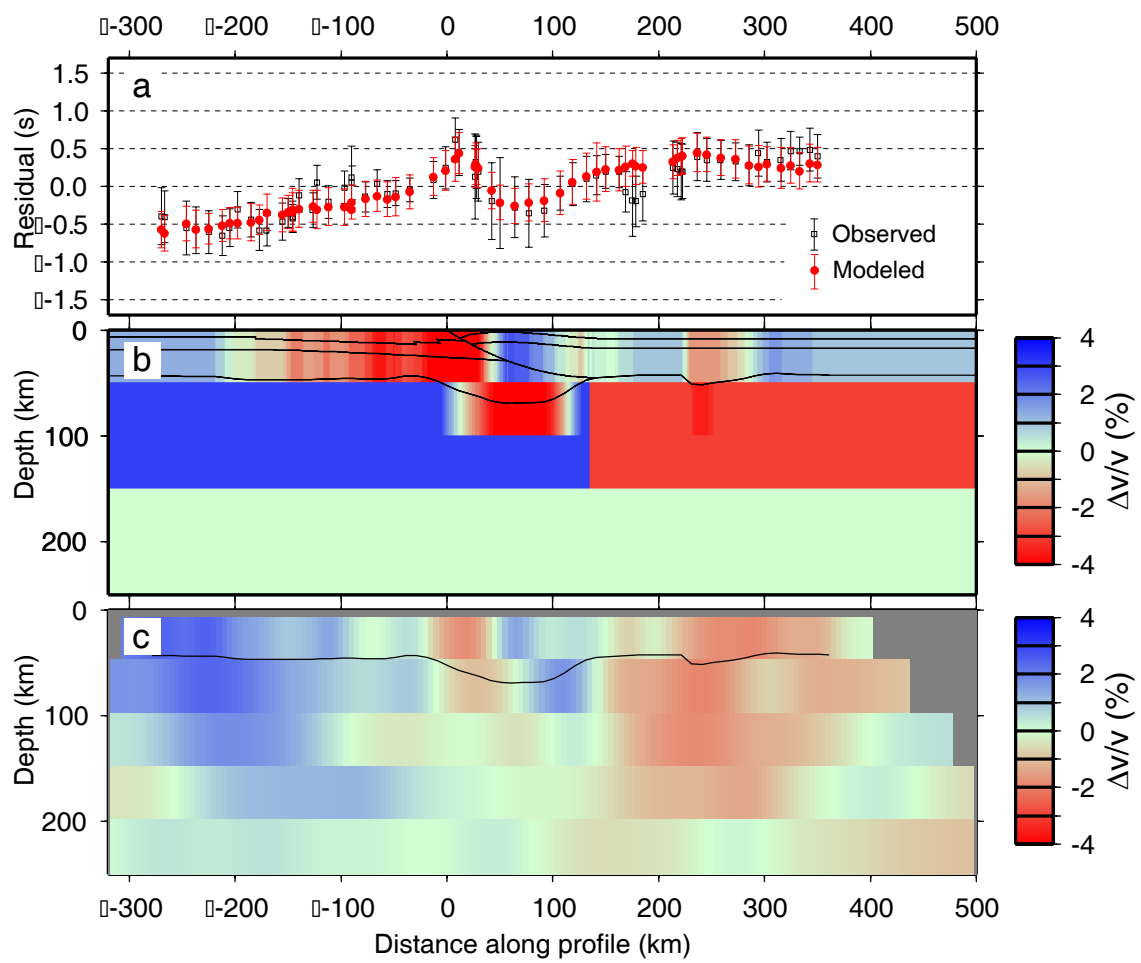


Figure 7

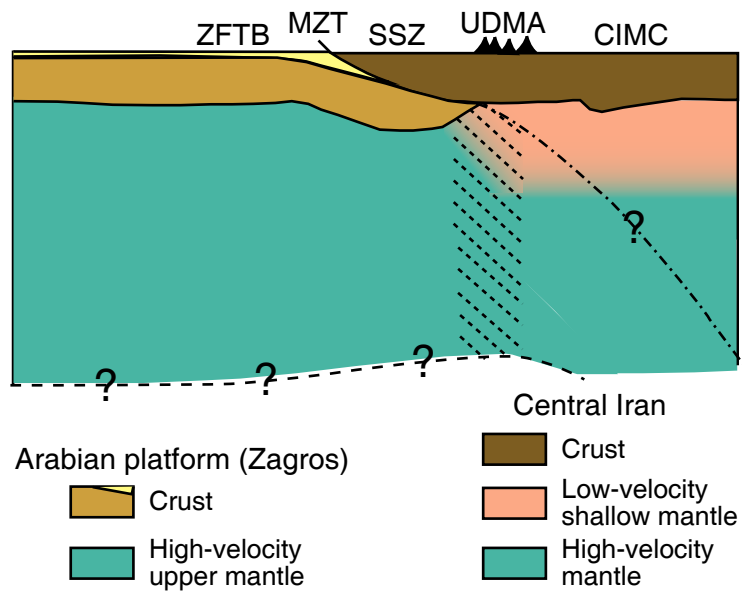


Figure 8